

The temporal limits of predicting fault failure

Kun Wang^{1,2*}, Christopher W. Johnson^{1*}, Kane C. Bennett¹, Paul A. Johnson¹

¹Los Alamos National Laboratory, Geophysics Group, Los Alamos, N.M.

²Center for Nonlinear Studies, Los Alamos National Laboratory, Los Alamos, NM, 87545, USA

Key Points:

- The limits of machine learning models are explored for predicting the future frictional behavior of laboratory earthquake slip
- A deep learning model is applied to acoustic emission data broadcast from the fault to predict future friction
- Acoustic emissions broadcast from the fault are found to carry information used for predicting future fault friction

Statement:

This manuscript is a non-peer reviewed preprint submitted to EarthArXiv.

*NOTE: KW and CWJ contributed equally to this paper

Corresponding author: Paul A. Johnson, paj@lanl.gov

15 **Abstract**

16 Machine learning models using seismic emissions can predict instantaneous fault
17 characteristics such as displacement in laboratory experiments and slow slip in Earth.
18 Here, we address whether the acoustic emission (AE) from laboratory experiments contains
19 information about near-future frictional behavior. The approach uses a convolutional encoder-
20 decoder containing a transformer layer. We use as input progressively larger AE input
21 time windows and progressively larger output friction time windows. The attention map
22 from the transformer is used to interpret which regions of the AE contain hidden information
23 corresponding to future frictional behavior. We find that very near-term predictive information
24 is indeed contained in the AE signal, but farther into the future the predictions are progressively
25 worse. Notably, information for predicting near future frictional failure and recovery are
26 found to be contained in the AE signal. This first effort predicting future frictional
27 behavior with machine learning will guide efforts for applications in Earth.

28 **Plain Language Summary**

29 Over the last 5 years it has been shown that machine learning is a powerful tool
30 to learn about the inside of faults from the acoustic emissions that the fault broadcasts.
31 For instance, the emissions can inform us of the instantaneous fault displacement and
32 friction in addition to timing of an upcoming earthquake in laboratory experiments as
33 well as for the phenomenon of slow slip in Earth. Here we show that by applying a deep
34 learning approach that has shown striking results in natural language processing and computer
35 vision, the seismic emissions also contain foreshadowing information about the immediate
36 future of fault friction. Remarkably, the emissions can tell us if the laboratory fault is
37 about to fail, and how it will begin to recover.

38 **Introduction**

39 Applying machine learning techniques to fault slip from laboratory shear experiments
40 has demonstrated that continuous acoustic/seismic signals emanating from an active fault
41 contain rich information regarding the instantaneous and future characteristics of that
42 system. The fault acoustic emissions are imprinted with information regarding its current
43 state and where it is in the slip cycle. Indeed, the statistical features of the continuous
44 seismic signal emitted from the fault and identified by the machine learning model allow
45 the prediction of instantaneous fault friction, displacement, fault gouge thickness, slip
46 velocity and the timing of the next laboratory earthquake ('labquake'), e.g., (Rouet-Leduc
47 et al., 2017, 2018; Lubbers et al., 2018; Hulbert et al., 2019, 2019; P. A. Johnson et al.,
48 2021; Wang et al., 2021). The labquake magnitude can also be predicted to a lesser degree,
49 and with considerably less precision and accuracy than quantities related to timing (Hulbert
50 et al., 2019).

51 Other model inputs such as seismic wave velocity, wave amplitude (Shokouhi et al.,
52 2021), and geodetic measurements (Corbi et al., 2019) have also been successfully applied
53 to predict instantaneous and future fault characteristics. Since the seminal paper first
54 describing machine learning model predictions by Rouet-LeDuc and colleagues (Rouet-
55 Leduc et al., 2017), many works now exist describing these behaviors—too many to reference
56 here. In addition, a Kaggle competition based on laboratory earthquake prediction was
57 also recently held where many hundreds of competitors took part in developing machine
58 learning models for predicting timing of the upcoming slip event (P. A. Johnson et al.,
59 2021).

60 In previous works, only predictions of the instantaneous characteristics and/or timing
61 (magnitude) of the next slip event were attempted. The question we address here is the
62 following—is there information contained in the continuous seismic signal regarding the

63 near future fault behavior including and beyond the next slip event? One might expect
 64 for instance, that due to a slip event the granular gouge is reset due to the intense, system
 65 wide perturbation associated with the labquake. We have observed previously that intense,
 66 externally applied dynamic perturbations—dynamic earthquake triggering—can have persistent
 67 impact through multiple slip cycles (P. A. Johnson et al., 2008). Such perturbations are
 68 considerably stronger than the seismic emission associated with the slip event however.
 69 Therefore it is unclear whether or not fault slip physical information can be carried within
 70 the fault gouge through a slip event into the next slip cycle.

71 Predicting future physical behavior in the form of bulk friction from current seismic
 72 emissions is the focus of this work. Such work will ultimately guide efforts in Earth to
 73 determine if there is near-term predictive information regarding fault physical characteristics
 74 such as displacement and earthquake timing contained in the continuous seismic emissions
 75 from active faults.

76 In the following, we describe the laboratory experiment and the accompanying data,
 77 and the deep learning modeling applied to those data. We then describe the prediction
 78 results and close with discussion of the results and conclusions.

79 **Methods**

80 **Deep Learning Model**

81 The deep learning model developed here for the future activity in the laboratory
 82 fault experiments is based on the Transformer architecture (Vaswani et al., 2017) designed
 83 as an encoder-decoder, or sequence-to-sequence, model that has shown remarkable results
 84 in natural language processing, computer vision, and time series modeling applications
 85 (Dosovitskiy et al., 2020; Li et al., 2019; Zhou et al., 2021). This particular model type
 86 was selected because the self-attention mechanism greatly improves the performance on
 87 sequential data compared to earlier designs that combine an attention model with recurrent
 88 neural networks such as Long Short-Term Memory or Gated Recurrent Units (Bahdanau
 89 et al., 2014; Luong et al., 2015). The success of the future prediction task relies on the
 90 ability of the Transformer model to learn a long-range dependency. Prior applications
 91 using Transformer models for long-sequence time-series forecasting have shown good results
 92 up to about 1000 future time points. These improvements rely on more efficient self-attention
 93 mechanisms such as LogSparse (Li et al., 2019) and ProbSparse (Zhou et al., 2021) that
 94 reduce computational complexity and memory usage.

95 In this work, the deep learning model is designed to predict the future friction coefficient
 96 as model output using as input acoustic emission (AE) obtained from laboratory biaxial
 97 shear data. Our approach uses a simplified version of the Transformer model that takes
 98 a time series vector as input and encodes it to a high dimensional representation of the
 99 signal that is then fed to the latent space tensor. The coefficients are passed through the
 100 Transformer and output to a second latent space. A decoder branch outputs friction coefficients
 101 at the corresponding future time step.

102 The first step is to design the input and output branches of the model as a convolutional
 103 encoder-decoder (CED) model and independently pre-train as an autoencoder (Figure
 104 1). The input-branch decoder is needed to obtain the embedding of the unit window of
 105 signals for a functional latent space. The output-branch encoder is needed for generating
 106 the target μ vectors for the teacher-forcing training stage of the Transformer. Note that
 107 the input decoder and the output encoder (the blocks in dashed lines in Figure 1) are
 108 not used in the Transformer model application, but only for model pre-training. Following
 109 the pre-training procedure, the parameters of the input and output CED models are fixed
 110 and the Transformer alone is trained using the future friction prediction data.

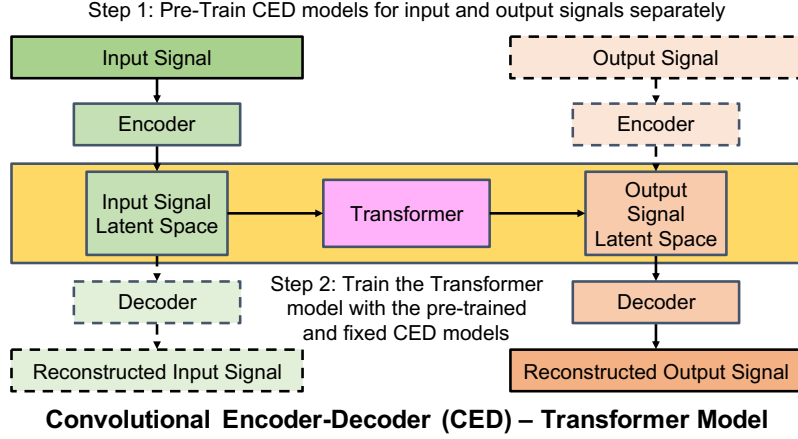


Figure 1: The deep learning model architecture used for pre-training and application to future predictions. The input signal (green column) and output signal (pink column) show the convolutional encoder-decoders that are connected by the Transformer via the latent space. The encoder consists of convolutional layers that take the input acoustic emission time series and map it into a sequence of vectors in a smaller space. The vectors are fed into a Transformer (yellow box) to predict output latent vectors and then to a decoder which transforms them into an output sequence with the target fault friction. The model components noted by the dashed lines are used in Step 1 for pre-training as an autoencoder to obtain the embedding vectors and not used in Step 2 with the Transformer for future predictions.

111 The latent vectors of the input AE signals are obtained by the pre-trained encoder
 112 model branch. For example, a total AE history of 2.56 s is encoded into a sequence of
 113 10 input latent vectors, each corresponding to 0.256 s windows of the input signal, with
 114 an embedding dimension of 64. The self-attention is the learned score representing the
 115 time-dependent relative importance of the input signal to the model for each prediction.
 116 The latent vectors are computed using a multi-head attention layer (Vaswani et al., 2017)
 117 in the Transformer’s encoder. These self-attention processed AE vectors are the keys and
 118 values to the multi-head attention in the Transformer’s decoder and the embedding vectors
 119 of the output μ generated in the past are the queries. The Transformer decodes to the
 120 next output embedding vector to match the target μ vector.

121 The approach applied here uses categorical predictions that represent different embedding,
 122 or latent, vectors from the groups of 256 signal data. This is analogous to translating
 123 input texts to output token IDs for natural language processing with a Transformer model
 124 except that here the dictionary terms are replaced with groups of 256 signal output data
 125 points. The alternative approach, which was tested during model development, is to predict
 126 embedding vectors of dimension 64 for a regression analysis. Hereafter, we refer to using
 127 the model to predict latent vectors of output friction coefficients as the regression approach
 128 and predicting category IDs of the outputs as the classification approach. The advantage
 129 of the classification approach is that the Transformer only needs to predict the probability
 130 logits, with the maximum value corresponding to the highest probability category. In
 131 the regression approach, alternatively, the Transformer needs to predict all dimensions
 132 of the latent vectors accurately to successfully estimate the output values. We obtain
 133 categories of the output embedding vectors through the Vector Quantised Variational
 134 AutoEncoder (VQ-VAE) (Oord et al., 2017) that learns a codebook of discrete vectors
 135 in the latent space. All continuous vectors after the convolutional encoder are compared
 136 against the codebook and the discrete latent vector with the smallest euclidean distance

137 is fed to the convolutional decoder. The codebook is updated by an exponential moving
 138 average (Oord et al., 2017) during the training stage. In a classification model the target
 139 categories are the discrete latent vectors of the codebook.

140 The model training is performed in 2 steps. In Step 1 the input and output CED
 141 branches are trained independently using the mean squared error (MSE) loss function
 142 between the target and reconstructed signal, plus the loss associated to the commitment
 143 loss in the VQ-VAE and the L2 regularization. In Step 2 the Transformer is trained using
 144 the classification approach for imbalanced data which focuses more on the categories that
 145 are difficult for the model to predict (Lin et al., 2017), since the number of values associated
 146 with the friction drops is much smaller than when the friction increases or is stable. Additionally,
 147 Step 2 is tested by training the Transformer using the regression approach with the MSE
 148 loss function between the target latent vectors of the output friction and the predicted
 149 vectors. In both training steps a batch size of 8 is used with the Adam optimizer and
 150 a custom learning rate scheduler. The training is terminated when the reconstruction
 151 loss on the validation data does not diminish for 50 epochs and the lowest validation loss
 152 is used for the final model.

153 Hyperparameter selection and model design optimization

154 Model hyperparameters and architecture are optimized for laboratory experiment
 155 p4677 data using a Bayesian optimizer (scikit-optimize package; Head et al., 2021) to
 156 train thousands of models with slightly different designs. Optimization is performed for
 157 the two CED models for embedding the input AE and output frictional coefficient, respectively,
 158 and the Transformer model for predicting future output embeddings. For the output CED
 159 model, the number of convolutional layers n_{out}^l , filter size f_{out} , kernel size k_{out} , the number
 160 of codes in the VQ-VAE’s codebook n_{out}^{vq} , the activation function act_{out} and the L2 regularization
 161 weight $l2_{out}$ are optimized. Similarly for the input CED model, n_{in}^l , f_{in} , k_{in} , n_{in}^{vq} , act_{in} ,
 162 and $l2_{in}$ are optimized. The hyperparameters for the Transformer include the number
 163 of encoder layers n_{enc}^{trsf} , the number of decoder layers n_{dec}^{trsf} , the number of attention heads
 164 n_{attn}^h , and the dropout rate r_{drop} (see Table S1). The search space is comprised of a range
 165 of values for each variable listed. The objective function for hyperparameter minimization
 166 is the MSE between the target future friction coefficients and the predicted frictions on
 167 the validation data of experiment No. p4677 using AE history of 2.56 s to predict 0.256
 168 s into the future. Each optimization attempt is run for 500 iterations, with the first 100
 169 iterations using random parameter selections. The procedure is distributed onto 16 GPUs
 170 with 5 processes running per GPU (80 models trained simultaneously) to rapidly test
 171 the search space. The procedure is iterated to adjust the search spaces until the final values
 172 are not at the boundary limits. The optimized hyperparameters for the final model design
 173 are provided in Supporting Information Table S1.

174 Laboratory experiment

175 We use laboratory data obtained from a bi-axial shear device. The device is a double-
 176 direct shear apparatus comprised of three blocks with two fault gouge layers, e.g., (Marone,
 177 1998; P. A. Johnson et al., 2013a; Rouet-Leduc et al., 2017; P. A. Johnson et al., 2021).
 178 The three block system is held in place by a fixed horizontal load, while the center block
 179 is driven by a piston oriented perpendicular to the horizontal load. The shear stress and
 180 friction on the gouge layers, from the center drive block and measured with a load cell,
 181 is an important experimental output. The simulated fault gouge comprises class IV spheres
 182 (dimension from 105–149 μm). The initial layer thickness is 2×4 mm (two layers), and
 183 the roughened interfaces with the drive block have dimensions 10 cm \times 10 cm. The drive
 184 block vertical displacement rate is 5 $\mu\text{m/s}$, corresponding to a strain rate of approximately
 185 1.2×10^{-3} /s. The apparatus is servo-controlled so that constant normal stress and displacement
 186 rate of the drive block are maintained at ± 0.1 kN and ± 0.1 $\mu\text{m/s}$, respectively. The apparatus
 187 is monitored via computer to record load on the drive block and drive block displacement

188 at 1 kHz. Once the system has been sheared to the point where it is in steady state conditions,
 189 the laboratory fault gouge layers fail in quasi-periodic cycles of stick and slip.

190 Laboratory Data Analysis

191 For the present analysis, experiment No. p4677 is used to train and validate the
 192 model, in which a fixed normal stress on the blocks of 2.5 MPa is maintained. Continuous
 193 AE broadcast from the fault zone were recorded via a Verasonics multichannel recording
 194 system and used as the input signal to the deep learning model, as described above. The
 195 coefficient of friction (μ) was used as the target output signal. The entire experiment p4677
 196 signals are split into 60% training and 40% validation data. These segments of signals
 197 are further split into sliding windows with the window size for inputs l_{in} , the window
 198 size for outputs l_{out} , the step size for the input windows l_{step} , and the lag between the
 199 start of the input and output windows l_{lag} . For the first step of training the CED models
 200 with instantaneous prediction data, $l_{in} = l_{out} = l_{step}$, $l_{lag} = 0s$, and l_{in} is equal to
 201 the unit window length (0.256 s in the Results) of signals embedded into one latent vector.
 202 For the second step of training the Transformer in the latent space with future prediction
 203 data while keeping the pre-trained CED fixed, l_{in} and l_{out} are no longer required to be
 204 the same, $l_{lag} = l_{in}$ and $l_{step} = l_{out}$ to ensure zero overlapping between input and output
 205 windows. The values of 0.256 s, 0.512 s, 1.024 s, 1.536 s, 2.048 s, 2.56 s are tested for l_{in}
 206 and l_{out} in order to study the window size effect on the prediction accuracy of the future
 207 fault slips. The size of the datasets depends on the above length hyperparameters. For
 208 example, for future prediction data with $l_{in} = 2.56s$, $l_{out} = 0.256s$, $l_{lag} = 2.56s$ and
 209 $l_{step} = 0.256s$, there are 694 pairs of input and output signal windows in the training
 210 dataset and 459 pairs in the validation dataset. Experiment No. p4581 is used as the
 211 testing dataset, in which progressively larger normal loads were applied and the steady
 212 states are at 3, 4, 5, 6, 7, 8 MPa normal stresses. In the following we focus on the 3MPa
 213 load analysis.

214 All input and output signals are normalized by subtracting the mean and dividing
 215 by the standard deviation using the statistics extracted from the training signal data.
 216 For the p4677 data, the statistics from the training signals are 8.878 ± 21.018 for the input
 217 AE signals and 0.652 ± 0.0413 for the output μ . When making predictions using experiment
 218 p4581 data with increasing normal loads, the statistics are extracted from the first 40%
 219 of the signals at each normal stresses for AE and 0.435 ± 0.024 for μ .

220 Results and Discussion

221 We first compared the future prediction accuracy between the classification approach
 222 and the regression approach, as well as between using the full waveform and AE magnitude
 223 signals as model inputs. We found classification outperforms regression and therefore will
 224 focus on these results. The optimal model we found was using the classification approach
 225 with the AE magnitudes as inputs after hyperparameter optimization (Table S1).

226 The future prediction accuracy using progressively increasing input and output window
 227 sizes on the validation and testing signals are tabulated in the matrix shown in Figure
 228 2. A larger matrix showing more window sizes is provided in Figure S1 of Supporting
 229 Information. The Mean Absolute Percent Error (MAPE) values are noted in the matrix
 230 figures for validation and testing, respectively. We note that average MAPE/MSE scores
 231 are not a perfect indicator of model performance; however, they do provide an indication
 232 of prediction accuracy (and are commonly applied metrics). The validation data set uses
 233 a portion of experiment p4677 data the model had not seen during training. The trained
 234 model is then applied to the p4581 testing data set for an experiment that were conducted
 235 at a slightly different load level (3 MPa vs. 2.5 MPa). The results show for the validation
 236 set that near-term predictions are about the same with the exception of the shortest window
 237 length. In contrast, the testing data shows degrading prediction as the input window length

238 increased beyond 2.048 s. Similarly, predictions further into the future degrade with window
 239 length. The best results for the training data are in the range of 1.024 - 2.048 seconds
 240 input and 0.256 s prediction window length. Predictions degrade with longer window lengths
 241 into the future. In summary, the model predictions are best for short future time sequences,
 242 and predictions beyond approximately 2.5 s are less good.

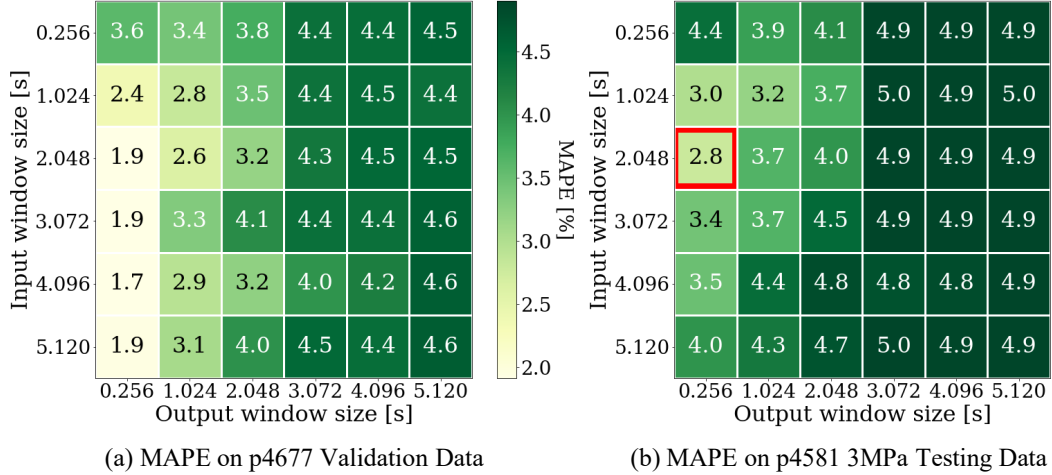


Figure 2: Grid search for 36 different input and prediction window lengths, showing MAPE of future predictions using different input/output window sizes. The validation data (left) is from experiment p4677, 2.5 MPa applied load data with 60%/40% train/validation split, and the testing data (right) are from the experiment p4581 dataset conducted at 3 MPa. The window highlighted with the red rectangle has the smallest testing data error and these model predictions are plotted in Figure 3. Supplementary matrices of MAPE results with finer window size (0.256 s step size) until 2.56 s is provided in Figure S1.

243 Figure 3 shows the predictions for the time window exhibiting the best MAPE—
 244 the matrix element denoted with the red box in Figure 2. Figure 4 shows predictions for
 245 the diagonal elements shown in the right panel in Figure 2. In Figure 3 one can see that
 246 the predictions are reasonably good overall. Many frictional failures are predicted, as are
 247 the succeeding recoveries. For some slip events, the event is not well predicted and the
 248 onset of recovery is therefore poorly predicted, e.g., events at approximately 44 and 54
 249 sec. Large precursors may be predicted (e.g., approximately 120 sec) or missed entirely
 250 (e.g., 15 sec). While a slip event may be predicted, the full friction failure magnitude is
 251 not as was observed in previous works applying many different models, e.g., (P. A. Johnson
 252 et al., 2021). In general the predictions improve through the slip cycle. The fact that
 253 the model is able to predict the failure event just before it takes place is encouraging.
 254 The onset of frictional recovery post-failure is also predicted in many cases suggesting
 255 there is knowledge contained in the AE regarding the onset of the future labquake cycle.
 256 The intense acoustic emission associated with the failure event apparently does not entirely
 257 erase fault system memory.

258 From the self-attention calculated in the Transformer latent-space, the relative importance
 259 of different parts of the AE input for future predictions can be analyzed by plotting the
 260 attention scores to visualize their distribution with respect to the AE history. The top
 261 panel of Figure 3 shows the mean attention scores and their standard deviation, computed
 262 from successive sliding input windows. The attention scores represent the average of the
 263 attention heads for a given input window. An expanded view of eight stress cycles is shown

264 in the lower panel to better visualize the variance in the signal and the accuracy of the
 265 friction predictions. Where the attention scores are largest indicates time intervals when
 266 the AE signal is most important for the future friction predictions. In general, the self
 267 attention scores indicate the model predictions are better in time intervals where impulsive
 268 precursors occur immediately preceding failure but also where the scores fluctuate the
 269 most.

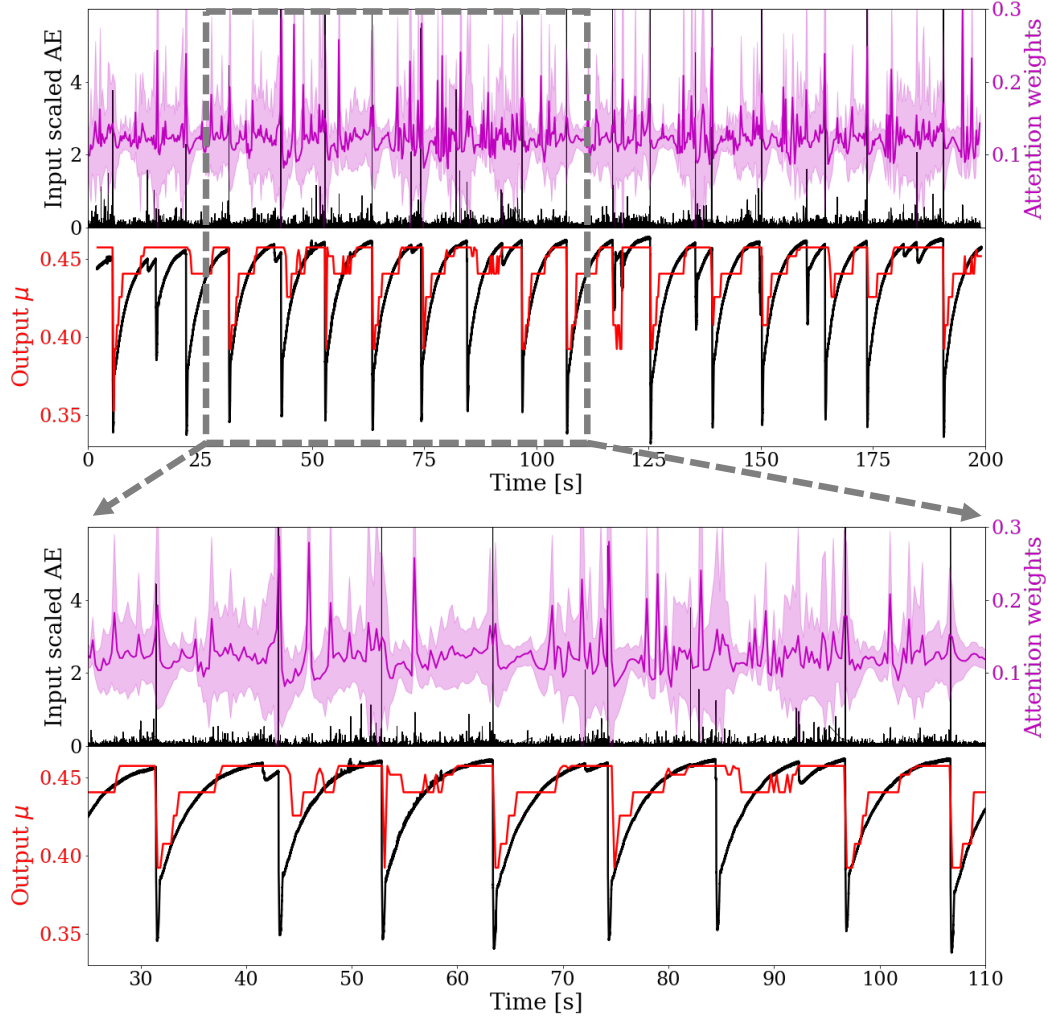


Figure 3: Attention scores shown with the AE and predicted friction values for the model shown in the red rectangle in Figure 2. In each figure the upper panel shows the mean attention score ± 1 standard deviation when predicting segments of 0.256 s window using 2.048 s history. The lower panel is the corresponding friction prediction. The bottom figure shows an expanded view from 25s to 110s to better highlight the time series details. In the 8 significant fault failures during this period, the timing of 5 failures are predicted at the correct time step, 2 are predicted after the slip event, and 1 is missed by the model.

270 The future predictions using the p4581 testing data for successively larger input
 271 and output windows as shown along the diagonal in the right panel in Figure 2 are presented
 272 in Figure 4. The time series data illustrate what the MAPE values listed in Figure 2 indicate.
 273 The 1.024 s input and output underscore the best prediction capability, and the prediction
 274 degrades progressively as the prediction time window size increases. Looking at the 0.256s

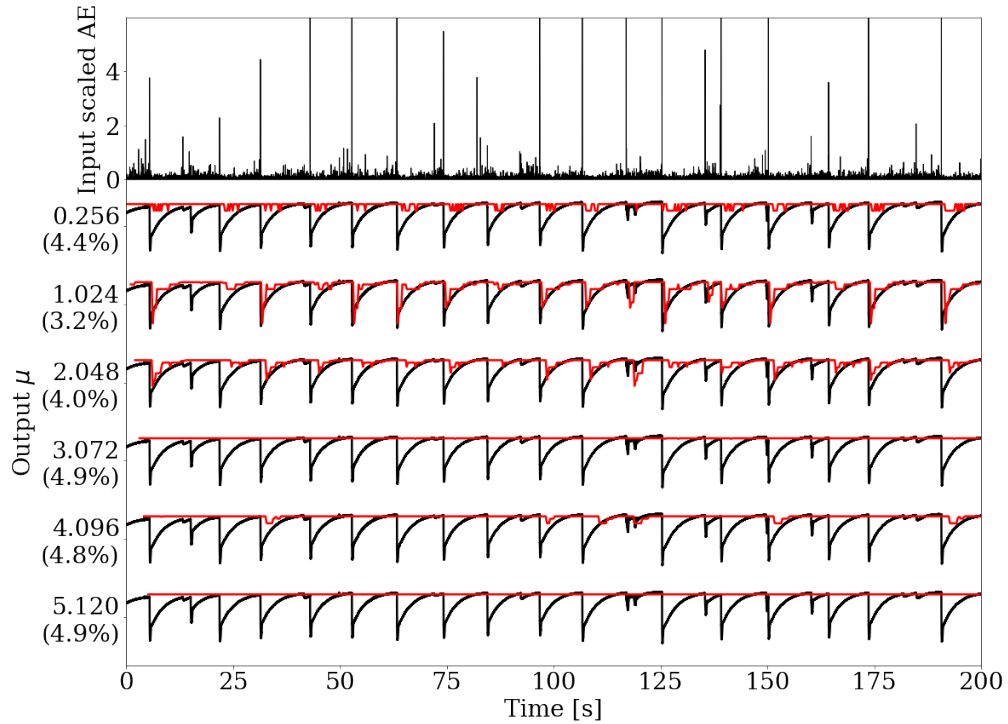


Figure 4: Test data (p4581) and the model predictions of the friction using equal length input and output window sizes (the diagonal of Figure 2b). The friction prediction is shown in red and the experiment measurements in black. The y-axis labels shows the input and output window lengths 0.256s, 1.024s, 2.048s, 3.072s, 4.096s, 5.12s and the MAPE error in parentheses. More prediction examples are provided in Supplementary materials Figure S2 and S3.

275 results the predictions are quite poor, possibly due to such a small input window size.
 276 For the time windows longer than 3 seconds there appears to be insufficient information
 277 contained in the AE signal to predict anything, but this also may reflect the model generalization.
 278 We note that poorer accuracy for longer window lengths could arise from the limitations
 279 of the Transformer model to capture long-term dependency in the latent space (embedding)
 280 of signals, although proven to be very successful in applications for natural language processing.

281 Previous work shows good instantaneous prediction capability contained in AE continuous
 282 waveforms. Signal energy was identified as key to instantaneous and time-to-failure prediction
 283 using both decision tree and deep learning models in the laboratory experiment data (e.g.,
 284 Rouet-Leduc et al., 2017; P. A. Johnson et al., 2021) and for slow slip in Earth (e.g., Hulbert
 285 et al., 2019; C. W. Johnson & Johnson, 2021). The analysis described here shows there
 286 is also information contained in the continuous signal regarding the immediate future
 287 behavior. The model attention scores focus on the region preceding frictional failure where
 288 precursors occur. This is logical near failure, based on our knowledge of classical seismic
 289 precursors in the laboratory (e.g., P. A. Johnson et al., 2013b) and those observed often,
 290 but not always, in Earth (Scholz, 2002; Bouchon et al., 2013). The results also indicate
 291 that within the inter-event portion of the earthquake cycle, near term friction prediction
 292 is also possible. Perhaps most interesting is that the seismic signal contains information
 293 predictive of the fault friction immediately beyond the failure event when one might expect
 294 the system to be unstable. The attention scores do not shed light as to why this is the
 295 case, but it is truly intriguing and future endeavors might provide clues as to what features
 296 of the signal contain this information. Applying machine learning approaches such as
 297 that described in this work, to continuous seismic signals as well as other geophysical data,
 298 will continue advancing our understanding of fault activity while advancing earthquake
 299 hazards assessment.

300 Acknowledgements

301 KW and PAJ acknowledge support by the U.S. Department of Energy, Office of
 302 Science, Office of Basic Energy Sciences, Chemical Sciences, Geosciences, and Biosciences
 303 Division under grant 89233218CNA000001. KW also acknowledges support by the Center
 304 for Nonlinear Studies (CNLS) at Los Alamos National Laboratory. CWJ and KCB acknowledge
 305 Institutional Support (Laboratory Directed Research and Development) at Los Alamos
 306 National Laboratory. The authors declare no competing interests. We thank Chris Marone
 307 for the laboratory data.

308 References

- 309 Bahdanau, D., Cho, K., & Bengio, Y. (2014). Neural machine translation by jointly
 310 learning to align and translate. *arXiv preprint arXiv:1409.0473*.
- 311 Bouchon, M., Durand, V., Marsan, D., Karabulut, H., & Schmittbuhl, J. (2013).
 312 The long precursory phase of most large interplate earthquakes. *Nature*
 313 *Geoscience*, 6. doi: 10.1038/ngeo1770
- 314 Corbi, F., Sandri, L., Bedford, J., Funicello, F., Brizzi, S., Rosenau, M., &
 315 Lallemand, S. (2019). Machine learning can predict the timing and size of
 316 analog earthquakes. *Geophysical Research Letters*, 46(3), 1303-1311. doi:
 317 10.1029/2018GL081251
- 318 Dosovitskiy, A., Beyer, L., Kolesnikov, A., Weissenborn, D., Zhai, X., Unterthiner,
 319 T., ... others (2020). An image is worth 16x16 words: Transformers for image
 320 recognition at scale. *arXiv preprint arXiv:2010.11929*.
- 321 Head, T., Kumar, M., Nahrstaedt, H., Louppe, G., & Shcherbatyi, I. (2021,
 322 October). *scikit-optimize/scikit-optimize*. Zenodo. Retrieved from
 323 <https://doi.org/10.5281/zenodo.5565057> doi: 10.5281/zenodo.5565057
- 324 Hulbert, C., Rouet-Leduc, B., Johnson, P. A., Ren, C. X., Rivière, J., Bolton,

- 325 D. C., & Marone, C. (2019). Similarity of fast and slow earthquakes
 326 illuminated by machine learning. *Nature Geoscience*, *12*(1), 69–74. doi:
 327 10.1038/s41561-018-0272-8
- 328 Johnson, C. W., & Johnson, P. A. (2021). Learning the low frequency earthquake
 329 daily intensity on the central san andreas fault. *Geophysical Research Letters*,
 330 *48*(15), e2021GL092951. doi: 10.1029/2021GL092951
- 331 Johnson, P. A., Ferdowsi, B., Kaproth, B. M., Scuderi, M., Griffa, M., Carmeliet,
 332 J., ... Marone, C. (2013a). Acoustic emission and microslip precursors to
 333 stick-slip failure in sheared granular material. *Geophysical Research Letters*,
 334 *40*(21), 5627–5631.
- 335 Johnson, P. A., Ferdowsi, B., Kaproth, B. M., Scuderi, M., Griffa, M., Carmeliet,
 336 J., ... Marone, C. (2013b). Acoustic emission and microslip precursors to
 337 stick-slip failure in sheared granular material. *Geophysical Research Letters*,
 338 *40*(21), 5627–5631. doi: 10.1002/2013GL057848
- 339 Johnson, P. A., Rouet-Leduc, B., Pyrak-Nolte, L. J., Beroza, G. C., Marone, C. J.,
 340 Hulbert, C., ... Reade, W. (2021). Laboratory earthquake forecasting:
 341 A machine learning competition. *Proceedings of the National Academy of*
 342 *Sciences*, *118*(5). doi: 10.1073/pnas.2011362118
- 343 Johnson, P. A., Savage, H. M., Knuth, M. W., Gombert, J., & Marone, C. (2008).
 344 Effects of acoustic waves on stick-slip in granular media and implications for
 345 earthquakes. *Nature*, *451*, 57–60.
- 346 Li, S., Jin, X., Xuan, Y., Zhou, X., Chen, W., Wang, Y.-X., & Yan, X. (2019).
 347 Enhancing the locality and breaking the memory bottleneck of transformer on
 348 time series forecasting. *Advances in Neural Information Processing Systems*,
 349 *32*, 5243–5253.
- 350 Lin, T.-Y., Goyal, P., Girshick, R., He, K., & Dollár, P. (2017). Focal loss for
 351 dense object detection. In *Proceedings of the IEEE International Conference on*
 352 *Computer Vision* (pp. 2980–2988).
- 353 Lubbers, N., Bolton, D., Mohd-Yusof, J., Marone, C., Barros, K., & Johnson, P.
 354 (2018). Earthquake catalog-based machine learning identification of laboratory
 355 fault states and the effects of magnitude of completeness. *Geophysical Research*
 356 *Letters*, *45*. doi: 10.1029/2018GL079712
- 357 Luong, M.-T., Pham, H., & Manning, C. D. (2015). Effective approaches to
 358 attention-based neural machine translation. *arXiv preprint arXiv:1508.04025*.
- 359 Marone, C. (1998). Laboratory-derived friction laws and their application to seismic
 360 faulting. *Annual Review of Earth and Planetary Sciences*, *26*(1), 643–696. doi:
 361 10.1146/annurev.earth.26.1.643
- 362 Oord, A. v. d., Vinyals, O., & Kavukcuoglu, K. (2017). Neural discrete
 363 representation learning. *arXiv preprint arXiv:1711.00937*.
- 364 Rouet-Leduc, B., Hulbert, C., Bolton, D. C., Ren, C. X., Riviere, J., Marone, C.,
 365 ... Johnson, P. A. (2018). Estimating fault friction from seismic signals
 366 in the laboratory. *Geophysical Research Letters*, *45*(3), 1321–1329. doi:
 367 10.1002/2017GL076708
- 368 Rouet-Leduc, B., Hulbert, C., Lubbers, N., Barros, K., Humphreys, C. J.,
 369 & Johnson, P. A. (2017). Machine learning predicts laboratory
 370 earthquakes. *Geophysical Research Letters*, *44*(18), 9276–9282. doi:
 371 10.1002/2017GL074677
- 372 Scholz, C. (2002). *The mechanics of earthquake faulting*. doi: 10.1017/
 373 CBO9780511818516
- 374 Shokouhi, P., Girkar, V., RiviĀšre, J., Shreedharan, S., Marone, C., Giles, C. L., &
 375 Kifer, D. (2021). Deep learning can predict laboratory quakes from active
 376 source seismic data. *Geophysical Research Letters*, *48*(12), e2021GL093187.
 377 doi: 10.1029/2021GL093187
- 378 Vaswani, A., Shazeer, N., Parmar, N., Uszkoreit, J., Jones, L., Gomez, A. N., ...
 379 Polosukhin, I. (2017). Attention is all you need. In *Advances in neural*

- 380 *information processing systems* (pp. 5998–6008).
- 381 Wang, K., Johnson, C. W., Bennett, K. C., & Johnson, P. A. (2021, 12). Predicting
382 fault slip via transfer learning. *Nature Communications*, *12*. doi: 10.1038/
383 s41467-021-27553-5
- 384 Zhou, H., Zhang, S., Peng, J., Zhang, S., Li, J., Xiong, H., & Zhang, W. (2021).
385 Informer: Beyond efficient transformer for long sequence time-series
386 forecasting. In *Proceedings of aaaa*.